

Statistical permutation quantifiers in the classical transition of conservative-dissipative systems

Gaspar Gonzalez^{1,2*}

Andrés M. Kowalski^{1,2}

¹*Instituto de Física de La Plata CONICET/UNLP, Buenos Aires, Argentina*

²*Comisión de Investigaciones Científicas (CIC), Argentina*

November 22, 2024

Abstract

We study the behavior of a nonlinear semiclassical system using Shannon entropy and two approaches to statistical complexity. These systems involve the interaction between classical variables (representing the environment) and quantum ones. Both conservative and dissipative regimes are explored. To calculate the information metrics, probability distributions are derived from the temporal evolution via the Bandt-Pompe permutation method. Additionally, we describe the classical limit in terms of a motion invariant linked to the uncertainty principle. Our analysis reveals three distinct regions, including a mesoscopic one, along with other notable findings.

Keywords: Nonlinear semiclassical systems, Shannon entropy, Statistical complexity, Bandt-Pompe method, Classical-quantum interaction, Mesoscopic regimes.

1 Introduction

The emergence of the classical world from the quantum domain is a topic of significant interest, both theoretically [1, 2, 3] and experimentally [4, 5, 6], as well as for its practical applications. The decoherence process [7], for instance, is closely linked to mesoscopic physics a field focusing on materials of intermediate scales. Mesoscopic systems, such as those used in nanotechnology, serve as practical examples [8, 9, 10, 11]. Additionally, semiclassical systems have been extensively employed over the years to address various physical problems [12, 13, 14, 15, 16, 17, 18, 19, 20, 21, 22, 23].

We have investigated systems that exhibit the coexistence of quantum and classical variables [24, 25, 26, 27, 28, 29, 30]. In these systems, the classical variables serve as a representation of the reservoir interacting with the quantum system.

Within this framework, we have explored the classical limit of quantum systems by employing a motion invariant associated with the Heisenberg Principle. Our approach includes dynamic analyses [24, 25, 26, 27, 28, 30] and the application of various tools from Information Theory (IT) [31, 32].

The classical limit of the system addressed in this work was previously examined in Ref. [30], utilizing Poincaré sections and analyzing the temporal evolution of key quantities. Both

*Corresponding author: gaspar.gonzalez@fisica.unlp.edu.ar

conservative and, for the first time, dissipative regimes were considered. In this study, we revisit the problem by employing Shannon entropy and two definitions of statistical complexity: the LMC complexity [33] and the Jensen-Shannon complexity [34]. To compute any information quantifier, a probability distribution function is required. For this purpose, we apply the Bandt-Pompe permutation based symbolic method [35], recognized for its efficiency in capturing key features of various time series [36, 37, 38, 39, 40, 41].

Our objective is to gain a deeper understanding and characterization of the process, uncovering details that cannot be obtained using dynamic tools alone.

2 The semi-classical model and classical limit

We consider a Hamiltonian of the form

$$\hat{H} = \frac{1}{2} \left(\omega_q (\hat{x}^2 + \hat{p}^2) + \omega_{cl} (A^2 + P_A^2) \hat{I} + e_q^{cl} A^2 \hat{x}^2 \right). \quad (1)$$

In this Hamiltonian, \hat{x} and \hat{p} are considered quantum operators while A and P_A canonically conjugated classic variables. \hat{I} is the Identity operator. ω_q and ω_{cl} are frequencies and e_q^{cl} a positive parameter positive [24]. The non-linear quantum-classical interaction appears through the term $e_q^{cl} A^2 \hat{x}^2$ in (1). The semiclassical methodology that we use, is developed in the Appendix. The equations of motion that govern the system, as demonstrated in Ref. [30], are given by the following set of coupled non-linear equations

$$\begin{aligned} \frac{d\langle \hat{x}^2 \rangle}{dt} &= \omega_q \langle \hat{L} \rangle, & \frac{d\langle \hat{p}^2 \rangle}{dt} &= -(\omega_q + e_q^{cl} A^2) \langle \hat{L} \rangle, \\ \frac{d\langle \hat{L} \rangle}{dt} &= 2(\omega_q \langle \hat{p}^2 \rangle - (\omega_q + e_q^{cl} A^2) \langle \hat{x}^2 \rangle), & \hat{L} &= \hat{x}\hat{p} + \hat{p}\hat{x} \\ \frac{dA}{dt} &= \omega_{cl} P_A, & \frac{dP_A}{dt} &= -A(\omega_{cl} + e_q^{cl} \langle \hat{x}^2 \rangle) - \eta P_A. \end{aligned} \quad (2)$$

To study the classical limit of the system (2), we need to compare with the solutions corresponding to the classical analogous of the Hamiltonian (1) [26]

$$H = \frac{1}{2} (\omega_q (x^2 + p^2) + \omega_{cl} (A^2 + P_A^2) + e_q^{cl} A^2 x^2). \quad (3)$$

By Hamilton's equations we obtain (see Appendix)

$$\begin{aligned} \frac{dx^2}{dt} &= \omega_q L, & \frac{dp^2}{dt} &= -(\omega_q + e_q^{cl} A^2) L, \\ \frac{dL}{dt} &= 2(\omega_q p^2 - (\omega_q + e_q^{cl} A^2) x^2), & L &= 2xp, \\ \frac{dA}{dt} &= \omega_{cl} P_A, & \frac{dP_A}{dt} &= -A(\omega_{cl} + e_q^{cl} x^2) - \eta P_A. \end{aligned} \quad (4)$$

We define I as

$$I = \langle \hat{x}^2 \rangle \langle \hat{p}^2 \rangle - \frac{\langle \hat{L} \rangle^2}{4} \geq \frac{\hbar^2}{4}. \quad (5)$$

I is a motion-invariant for the systems (2) in both regimens (conservative and dissipative) (see [24, 30]) and is related to the uncertainty principle describing the deviation with respect to classicity, a condition characterized by $I = x^2 p^2 - L^2/4 = 0$ (trivial motion-invariant).

Eqs. (2) do not explicitly depend upon \hbar while mean values depend on it via the initial conditions through I satisfying (5). The inequality (5) and its classical value, are crucial in our

study of the classical limit $I \rightarrow 0$, as will be seen throughout the article. Focus now attention upon the relative energy E_r .

$$E_r = \frac{|E|}{I^{1/2}\omega_q}, \quad (6)$$

where $E = \langle H \rangle$ is the total energy. E_r is also a motion invariant that verifies $E_r \geq 1$ due to the uncertainty principle. $E_r = 1$ corresponds to the minimum value and represents the totally quantum case. E_r is dimensionless. The LC is $I \rightarrow 0$, i.e.,

$$E_r \rightarrow \infty. \quad (7)$$

In the dissipative case we replace, in (6), E by $E(0)$ [30]. Our main interest lies in the evolution of observable when E_r grows from its minimum unity value $E_r = 1$.

3 Bandt-Pompe method

To calculate our Information quantifiers, it is necessary to have a probability distribution associated with the data series that one wants to analyze. In this case, of a time series of the semiclassical and classical systems. We obtain this probability distribution function (PDF) using the Bandt and Pompe method [35]. This methodology basically consists of a symbolization process that is described as follows: Let $\{x_t\}_{t=1,2,\dots,N}$ be an arbitrary time series, the first step is to divide the time series into $n = N - (d - 1)\tau$ overlapping partitions comprising $d > 1$ observations separated by $\tau \geq 1$ time units. For given values of d and τ , each data partition can be represented by

$$w_p = (x_p, x_{p+\tau}, x_{p+2\tau}, \dots, x_{p+(d-2)\tau}, x_{p+(d-1)\tau}), \quad (8)$$

where $p = 1, 2, \dots, n$ is the partition index. The parameters d and τ are the so-called embedding dimension and the embedding delay, respectively, the only two parameters of the Bandt and Pompe method. The original proposal presented by Bandt and Pompe was limited to $\tau = 1$, this means that the data partitions comprised consecutive elements of time series, however, Cao et al. [42], Zunino et al. [43] and Pessa and Ribeiro [44], studied the embedding delay for values greater than 1.

Then, for each partition w_p we evaluate the permutation $\pi_p = (r_0, r_1, \dots, r_{d-1})$ of the index numbers $(0, 1, \dots, d - 1)$ which arranges the elements of w_p in ascending order, that is, the permutation of the index numbers defined by the inequality $x_{p+r_0} \leq x_{p+r_1} \leq \dots \leq x_{p+r_{d-1}}$. In case of equality of values, the order of appearance of the elements of the partition is maintained, i.e., if $x_{p+r_{k-1}} = x_{p+r_k}$, then $r_{k-1} < r_k$ for $k = 1, \dots, d - 1$. After evaluating the permutation symbols associated with all data partitions, a symbolic sequence $\{\pi_p\}_{p=1,2,\dots,n}$ is obtained.

The ordinal probability distribution $P = \{p_i(\Pi_i)\}_{i=1,2,\dots,n_\pi}$ is the relative frequency of all possible permutations within the symbolic sequence

$$p_i(\Pi_i) = \frac{\text{number of partitions of type } \Pi_i \text{ in } \{\pi_p\}}{n}. \quad (9)$$

Here Π_i represents each of the $n_\pi = d!$ different ordinal patterns.

The Bandt Pompe method has desirable features (i) simplicity, (ii) extremely fast calculation-process, and (iii) robustness. It is also invariant with respect to non-linear monotonous transformations. This method can be applied to any type of time series (regular, chaotic, noisy, or experimental) [31].

4 Information Quantifiers

4.1 Shannon permutation entropy

The Shannon permutation entropy is defined as follows

$$S(P) = - \sum_{i=1}^{n_\pi} p_i(\Pi_i) \log p_i(\Pi_i), \quad (10)$$

where the probability distribution $P = \{p_i(\Pi_i)\}_{i=1,2,\dots,n_\pi}$ is obtained using the Bandt and Pompe method. Permutation entropy quantifies the randomness in the ordering dynamics of a time series. This means that $S = 0$ implies completely regular behavior, while $S = \log(n_\pi)$ indicates behavior with maximum disorder [35, 44].

The normalized permutation entropy adopts the form

$$H(P) = \frac{S(P)}{S_{\max}}, \quad (11)$$

where $S_{\max} = \log(n_\pi)$ y $0 \leq H \leq 1$.

4.2 LMC-statistical complexity

In 1995, Lopez-Ruiz, Mancini and Calbet (LMC) [33, 45], proposed a measure of complexity given by the following expression

$$C = H(P) \cdot D(P, P_e), \quad (12)$$

where $D(P, P_e) = \sum_{i=1}^{n_\pi} (p_i - 1/n_\pi)^2$ is known as the disequilibrium factor and is defined as a distance (Euclidean or 2-norm distance) between a probability distribution P and the equiprobable distribution P_e , with $P_e = \{1/n_\pi\}_{i=1,2,\dots,n_\pi}$. Disequilibrium gives us a way to measure how “separate” the probability distribution of the system under treatment is from the uniform distribution, which gives us maximum uncertainty of the state of the system.

4.3 Jensen Shannon-statistical complexity

The Jensen Shannon-statistical complexity (JSC) [34] is based on the pioneering Statistical complexity of López-Ruiz et al. The fundamental difference between these two quantities lies in how distances are measured in the probability space. The JSC is defined as the product of the permutation entropy and the Jensen-Shannon divergence between the ordinal distribution $P = \{p_i(\Pi_i)\}_{i=1,2,\dots,n_\pi}$ and the uniform distribution $P_e = \{1/n_\pi\}_{i=1,2,\dots,n_\pi}$ instead of Euclidean distance. We also consider the normalized version of the JSC.

$$C = \frac{H(P) \cdot D_{JS}(P, P_e)}{D^{\max}}, \quad (13)$$

where

$$D_{JS}(P, P_e) = S \left[\frac{1}{2} (P + P_e) \right] - \frac{1}{2} S(P) - \frac{1}{2} S(P_e), \quad (14)$$

is the Jensen-Shannon divergence [46] and

$$D^{\max} = -\frac{1}{2} \left[\frac{n_\pi! + 1}{n_\pi!} \log(n_\pi! + 1) - 2 \log(2n_\pi!) + \log(n_\pi!) \right], \quad (15)$$

is a normalization constant.

The Jensen Shannon statistical complexity is capable of capturing essential details of the dynamics, is an intensive quantity, and is capable of discerning between different degrees of periodicity and chaos [31, 46, 47, 48].

5 Results

To solve the equations (2) and (4) we choose the following parameter values: $\omega_q = \omega_{cl} = e_q^{cl} = 1$. While for the initial conditions we take $\langle \hat{L} \rangle(0) = L(0) = A(0) = 0$.

For the conservative system ($\eta = 0$), we choose $E = 0.6$. In the dissipative regimen we take the same value for the initial energy value $E(0) = 0.6$. In both regimes we fixed this values, as we set $I \rightarrow 0$ ($E_r \rightarrow \infty$) in (6). In the dissipative cases is $\eta = 0.05$.

We select $\langle \hat{x}^2 \rangle(0) = E/\omega_q - 0.98\sqrt{(E/\omega_q)^2 - I_L}$, where $I_L = I + \langle L \rangle(0)^2/4$. For the classic case is $x^2(0) = 0.02E/\omega_q$, which results from taking the value $I = 0$ in the previous expression. By appeal to (5) we see that $\langle \hat{p}^2 \rangle(0) = \frac{I}{\langle \hat{x}^2 \rangle}(0)$ ($p^2 = 0$ in the classical instance). In addition, from (1) we deduce $P_A(0)$ via

$$P_A = \frac{\pm}{\omega_{cl}^{1/2}} \sqrt{2E - \omega_q(\langle \hat{p}^2 \rangle + \langle \hat{x}^2 \rangle) - e_q^{cl} A^2 \langle \hat{x}^2 \rangle - \omega_{cl} A^2},$$

evaluating all quantities at the initial time. We have also an equivalent expression for the classical analogous system.

In the numerical calculation of the Shannon permutation entropy and the statistical complexities, the Python package `ordpy` developed by Arthur A. B. Pessa and Haroldo V. Ribeiro [44] was used. We have employed the values $d = 5$ and $\tau = 1$ for the dimensional embedding and embedding delay, respectively. The results have been conceptually confirmed using $d = 6$.

The time series for the semiclassical case, have been constructed with the values of $\langle \hat{x}^2 \rangle(t)$, each one for a different value of E_r (or I). Also we have considered in the classical scenario ($I = 0$), the unique series formed by the $x^2(t)$ values. In both cases to we have taken $N = 20000$ points for each series. The condition $N \gg d! = 120$ is verified [31].

In all figures we observe low values of the information quantifiers, unlike what we have found for the chaotic Hamiltonian of Refs. [31, 32]. This feature are consistent with the regularity observed in the Poincaré Sections [30]. In detail, after the jump observed in the quasi-quantum zone between $E_r \approx 1$ and $E_r \approx 2.8$ (see below), one finds a very small band of variation of the values. However, the three regions of Refs. [31, 32] of the path to the classical analogous, continues being observed (quasi-quantum, transitional and classical).

It is convenient an analysis with additional tools such as information quantifiers, which, as mentioned, have proven efficiency for this type of problem.

In Fig.1 we plot the normalized Entropy H vs. the relative energy E_r , for both conservative and dissipative regimes. In the conservative case (blue curve), between $E_r \approx 1$ and $E_r \approx 2.8$, we find out a zone, what we can call quasi-quantum. In the zone $E_r \approx 1$, with dynamic tools, quasi-periodic behavior has been observed (remember that $E_r = 1$ is the lowest possible value of E_r and corresponds to the fully quantum case). At $E_r \approx 2.8$ (first gray colored vertical dashed line), we have observed on a logarithmic scale, a drastic change (taking into account the mentioned small band of variation of H). The transition zone (mesoscopic) can be set between the values $E_r \approx 2.8$ and $E_r \approx 104.8$ and finally the convergence zone to the classical analogous value $H_c^{cl} = 0.1768$, can be seen from $E_r \approx 104.8$ (second gray discontinuous vertical line).

The equivalent zones corresponding to the dissipative regime (orange curve) are: quasi-quantum from $E_r \approx 2.8$ to $E_r \approx 3.6$ (first plum colored vertical dashed line), the transitional from $E_r \approx 3.6$ to $E_r < 123.0$, and the convergence zone to the analogous classic case from $E_r = 123.0$ (second plum colored vertical dashed line). $H_d^{cl} = 0.1720$, is the value of the entropy of the classical analogous in the dissipative case (remember that in this regime we replace in (6), E by $E(0)$).

Additionally, the figure contains an inset in which the morphology of the curves in the transition zone is observed in detail. This region can be associated with a mesoscopic one, due

to the important presence of quantum features. The zone of convergence to the totally classical system must correspond to a decoherence process [29].

In Figs. 2 we plot the two definitions of the statistical complexity vs. E_r . In both figures, one can clearly notice the three zones mentioned in Fig.1. These results are the same for both C_{JS} and C_{LMC} . The blue curve corresponds to the conservative case and the orange curve to the dissipative one. The dashed vertical lines indicate the transition zone, gray for the conservative regime (between $2.8 < E_r < 104.8$) and plum for the dissipative case (from $E_r > 3.6$ to $E_r < 123.0$). Furthermore, in each graph there is a inset that basically consists of an increase in scale of the original graph, showing the transition zone. In Figure 2a we can see the statistical complexity of Jensen-Shannon C_{JS} . $C_c^{cl} = 0.16401$ and $C_d^{cl} = 0.16058$ are the statistical complexity values of the classical analogous of the conservative and dissipative regimes, respectively. Figure 2b presents the statistical complexity introduced by Lopez-Ruiz et al. C_{LMC} vs E_r . The blue and the orange curves are associated to the conservative and dissipative system, respectively. In this case, $C_c^{cl} = 0.13533$ and $C_d^{cl} = 0.13426$ are the values of the statistical complexity of the classical analogous (conservative and dissipative regimen).

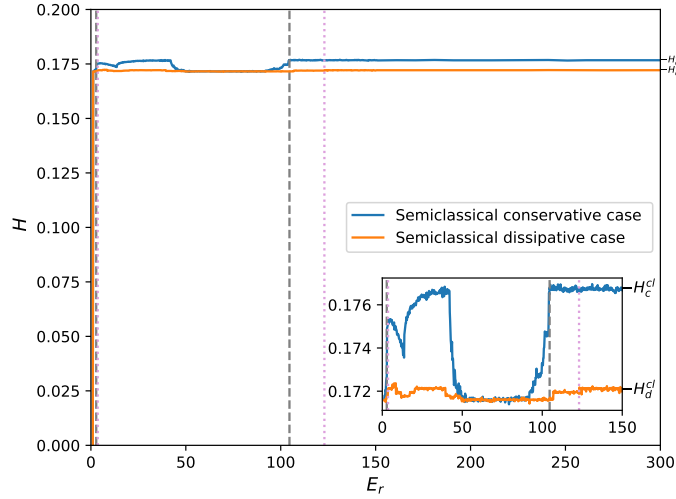
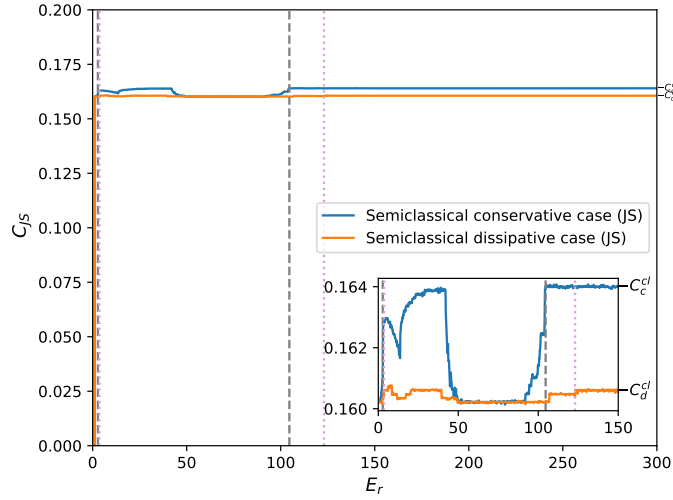
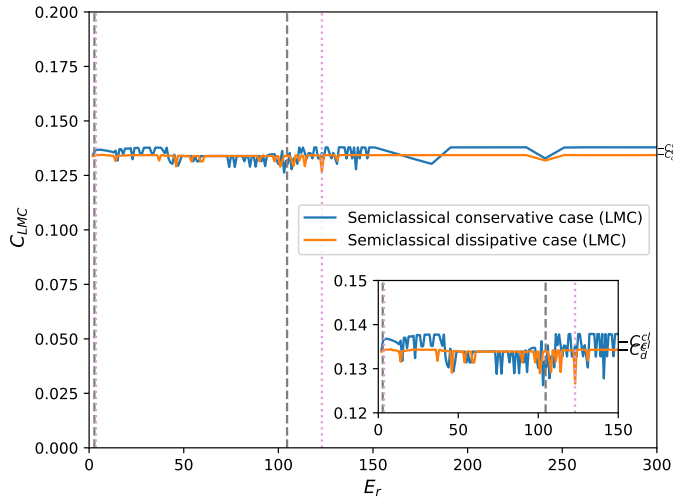


Figure 1: Normalized Shannon permutation entropy H as a function of the relative energy of the system E_r . The insets on the right are an up-scaling of the original graph, showing the transitions zones with more details. The blue curve corresponds to the entropy of the conservative case an the orange to the dissipative one. $H_c^{cl} = 0.17676$ and $H_d^{cl} = 0.17207$ are the corresponding entropies of the classical analogous in both regimes. Vertical lines indicate the transition zone, between quasi-quantum and classical zones. Dashed gray for the conservative system ($2.8 < E_r < 104.8$) and dotted plum for the dissipative one ($3.6 < E_{r0} < 123.0$).



(a)



(b)

Figure 2: We plot the two definitions of the statistical complexity vs. E_r . As in previous figure, vertical lines indicate the transition zone, between quasi-quantum and classical zones. Dashed gray for the conservative dynamics ($2.8 < E_r < 104.8$) and dotted plum for the dissipative one ($3.6 < E_{r_0} < 123.0$). The intervals are the same as in the case of entropy. In the insets we can see the transition zones in detail. The blue curves correspond to the conservative regime and the orange curves to the dissipative one. (a) Statistical complexity C_{JS} vs E_r . $C_c^{cl} = 0.16401$ and $C_d^{cl} = 0.16058$ are the statistical complexity values of the classical analogous in both conservative and dissipative cases, respectively. (b) Statistical complexity C_{LMC} vs E_r . $C_c^{cl} = 0.13533$ and $C_d^{cl} = 0.13426$ are the corresponding statistical complexity values of the classical analogous (conservative and dissipative regimes).

5.1 Comparing outcomes.

As we have already commented, all figures show convergence towards the values of the corresponding classical analogous. Except for fluctuations, in general the results corresponding to the conservative regime are slightly higher than those of the dissipative regime. A result that can be expected since the dynamics of the system is regular in both regimes. However, contrary to what one might think a priori, convergence start earlier in the conservative case. The zones are the same for the entropy H and the complexities C_{JS} and C_{LMC} . Transitional zone of the conservative regime is ($2.8 < E_r < 104.8$), while for the dissipative case it is ($3.6 < E_r < 123.0$).

Note that the representative figures of H and C_{JS} are similar but with a difference in scale. This is because the disequilibrium remains almost constant around its mean value $D_{JS} \approx 0.92985$ (conservative) and $D_{JS} \approx 0.93337$ (dissipative), for all values of E_r . In the case of the complexities C_{LMC} , the disequilibrium is also quasi-constant as a function of E_r , but it has greater fluctuations around its mean value $D_{LMC_c} \approx 0.76944$ and $D_{LMC_d} \approx 0.77906$ (conservative and dissipative dynamics).

Figures 3a and 3b are comparative graphs between C_{LMC} and C_{JS} for both regimes. The behavior of the curve of C_{LMC} is more erratic than the C_{JS} one (due to D_{LMC_c} and D_{LMC_d} behaviours). This happens for both the conservative and dissipative systems. On the other hand, the different criteria used to normalize the disequilibrium in the expressions of C_{LMC} and C_{JS} cause a difference in scale. Figures 4a and 4b, expose this characteristic for the conservative and dissipative regimes, respectively. To achieve a meaningful comparison, it was convenient to apply a translation to the complexity C_{LMC} by multiplying all values of the curve by the factor 1.196. It is observed that, despite the marked fluctuations in the amplitude of C_{LMC} compared to C_{JS} , both exhibit a similar profile. This phenomenon highlights the consistency in the underlying behavioral pattern.

In Figures 5 and 6 we represent the Poincaré sections (conservative regime) and the projections of the Poincaré sections (dissipative dynamics) (for more details see [30]), suitable for the results obtained in this work.

In Figure 5 we plot Poincaré sections corresponding to (a) $E_r = 1.000001$ and (b) $E_r = 1.02$, both in the semiquantum zone, (c) $E_r = 24.24$ belonging to the transition zone, (d) $E_r = 104.6$, the critical point between the transition and classical zones where convergence begins, (e) $E_r = 4 \cdot 10^4$ in the classical zone. Finally in (f) we depict the Poincaré section of the conservative classical analogous.

Figure 6 shows the projections of the 3D dissipative Poincaré sections, for the same E_r values in the same zones as figure 5 ([30]), in subfigures (a), (b), (c) and (e). Subfigure (d) correspond to the critical point for the dissipative regime $E_r = 123.0$. In (f) we plot the projection of the 3D Poincaré section of the dissipative classical analogous.

It is important to observe in these figures the difficulty in precisely defining, using Poincaré Sections, the limit between the three zones. This happens because of the system dynamics is very regular. However, the information quantifiers used in this work offer better differentiation.

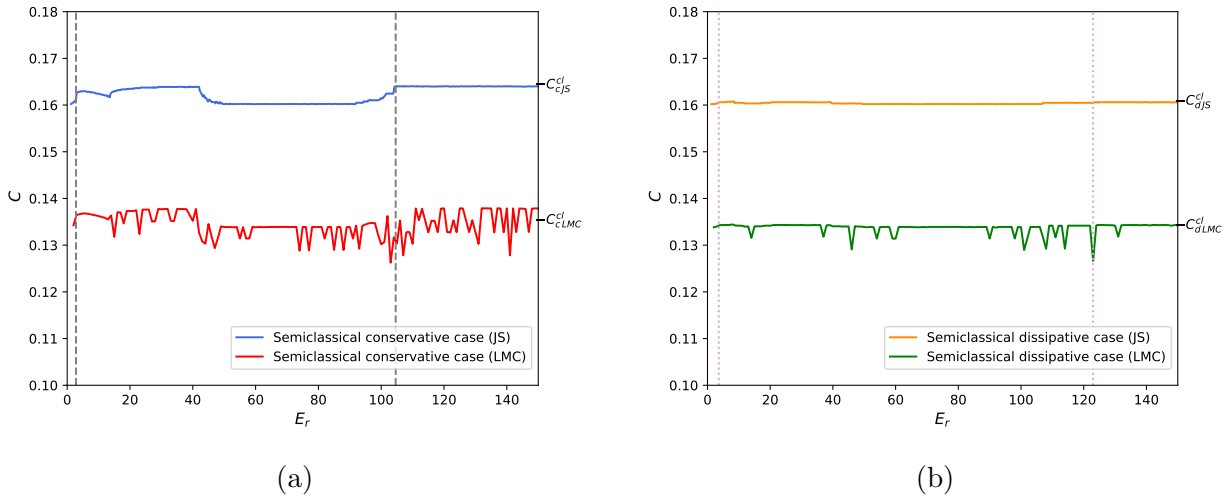


Figure 3: Comparative figure between C_{LMC} and C_{JS} as a function of the relative energy E_r . (a) Conservative dynamics. The blue and red curves exhibit the Jensen-Shannon and Lopez-Ruiz et al. statistical complexities, respectively. The gray dashed vertical lines indicate the transition zone (between $2.8 < E_r < 104.8$). (b) Dissipative case. The orange and green curves display the Jensen-Shannon and Lopez-Ruiz et al. complexities, respectively. The plum colored vertical dashed lines indicate the transition zone ($3.6 < E_{r_0} < 123.0$). In addition to the fluctuations of C_{LMC} , these plots show a difference in scale between both complexities. This is due to the differences between the normalization of the Jensen-Shannon divergence and the Lopez-Ruiz et al. disequilibrium.

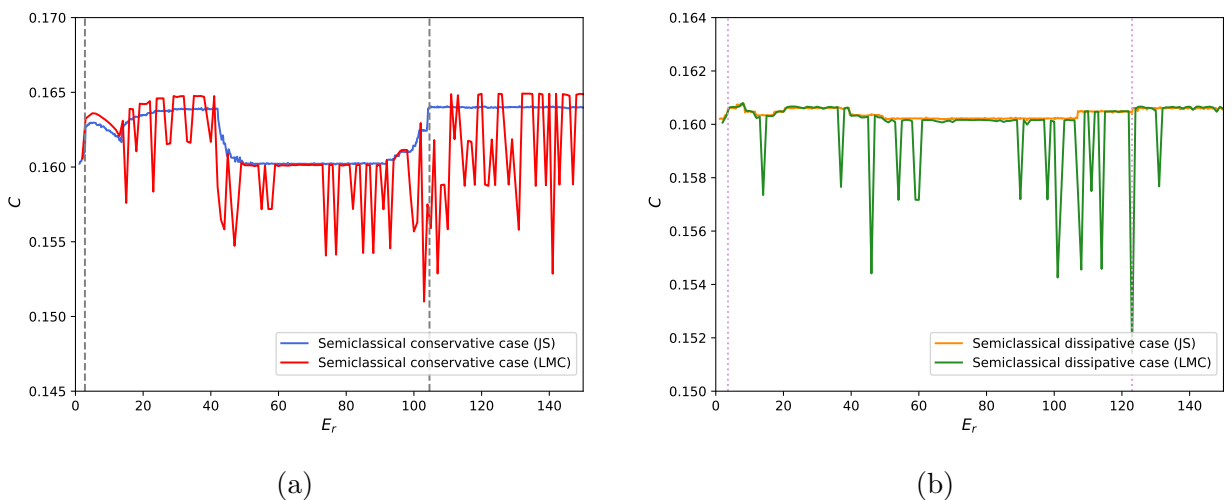
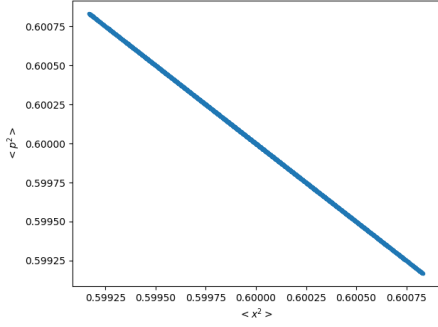
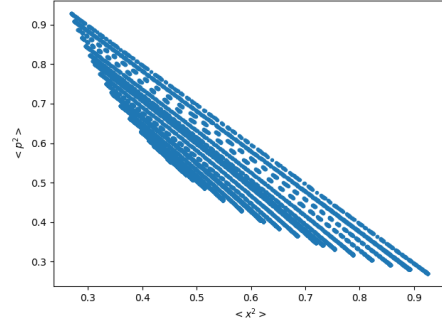


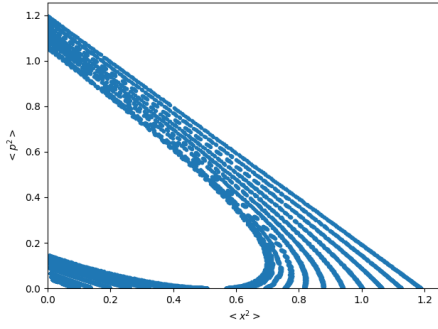
Figure 4: Comparative figure between C_{LMC} and C_{JS} vs. E_r . In this case we have changed the scale of C_{LMC} by a factor of 1.196. (a) Conservative regime and (b) dissipative one.



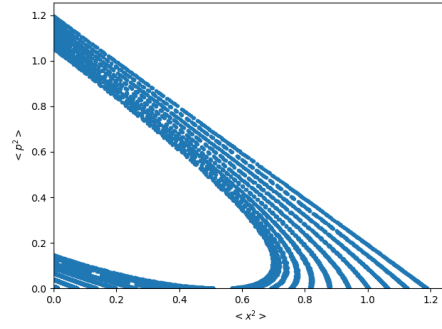
(a) $E_r = 1.000001$ (quasi-quantum zone).



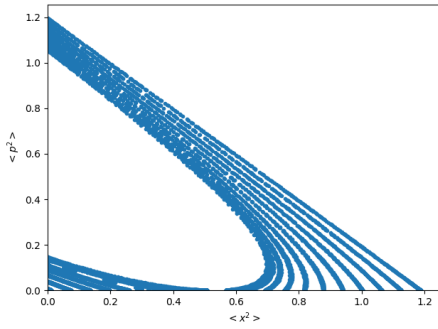
(b) $E_r = 1.02$ (quasi-quantum zone).



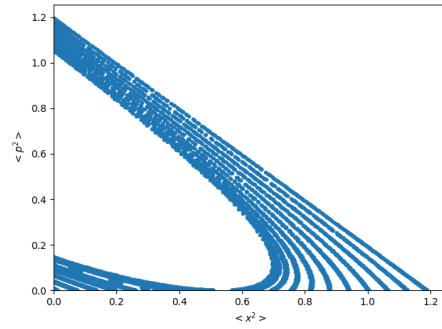
(c) $E_r = 24.24$ (transitional (mezoscopic zone)).



(d) $E_r = 104.6$ (critical point when convergence begins).

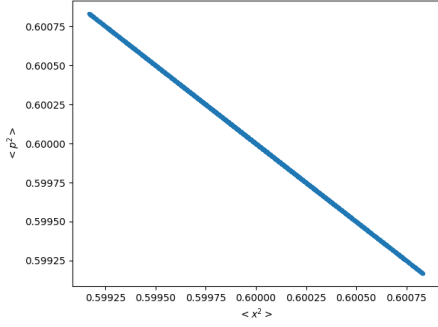


(e) $E_r = 4 \cdot 10^4$ (classical zone).

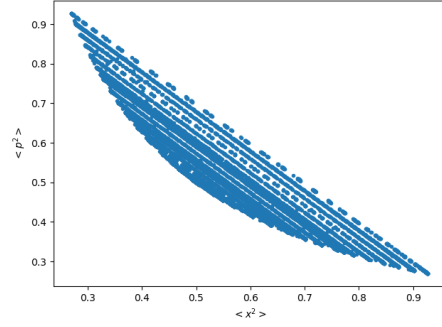


(f) $E_r = \infty$ (classical analogous).

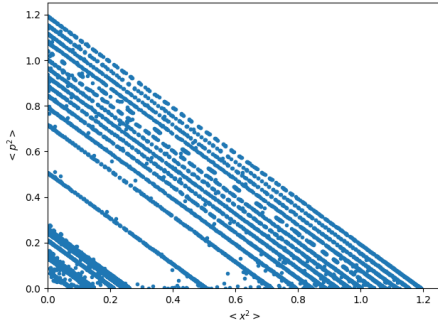
Figure 5: Poincaré sections corresponding to the conservative dynamics.



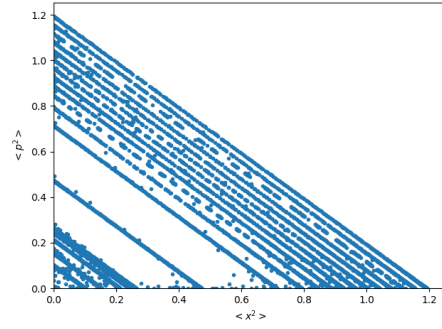
(a) $E_r = 1.000001$ (quasi-quantum zone).



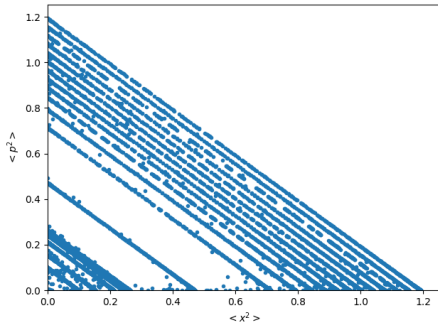
(b) $E_r = 1.02$ (quasi-quantum zone).



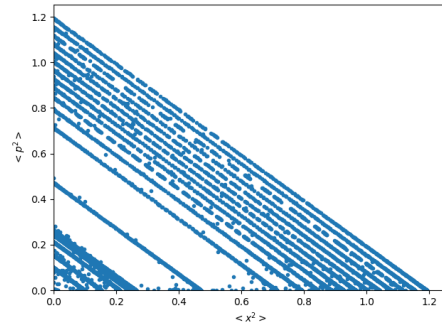
(c) $E_r = 24.24$ (transitional (mesoscopic zone)).



(d) $E_r = 123.0$ (critical point when convergence begins).



(e) $E_r = 4 \cdot 10^4$ (classical zone).



(f) $E_r = \infty$ (classical analogous).

Figure 6: Projections of the 3d Poincaré sections corresponding to the dissipative case.

6 Conclusions

In this article we have analyzed the conservative and dissipative dynamics of the semiclassical Hamiltonian (1), which contains both quantum and classical variables. For this we have used information quantifiers, such as the Shannon entropy H and the Statistical complexity. In the case of the latter, we analyze two versions, the pioneer one introduced by Lopez-Ruiz et al. C_{LMC} [33, 45] and the Jensen Shannon complexity C_{JS} [34]. The probability distribution to evaluate all these quantities was extracted from the time series using the Bandt and Pompe permutational method [35]. A methodology that has proven to be robust and reliable. In particular we have studied the classical limit of the system, that is, the convergence to the classical analogue of H represented by Eq. (3) (only with classical variables), as a function of the relative energy E_r (6), related to the Uncertainty Principle, with $E_r \rightarrow \infty$.

In [30] we had studied the same problem, but using dynamic tools such as Poincaré sections and projections of 3D Poincaré sections. The result found was the existence of three zones, quasi-quantum, transitional and finally one where the convergence to the results corresponding to the classical analogue was observed (classical zone). However, the boundaries between zones were diffuse, because the dynamics of the system is regular (see figures 5 and 6). The regularity of the dynamics is reflected in the figures of the present article, by their low values of all information quantifiers. Moreover, after the jump observed in the quasi-quantum zone, one finds a very small band of variation of the respective values.

It is seen in Figs. 1, 2, 3 and 4 that the Shannon permutation entropy H and the statistical complexities C_{LMC} and C_{JS} confirm the mentioned three zones of the process (quasi-quantum, transitional or mesoscopic and that of decoherence, convergent to the classical analogous result). The corresponding intervals of E_r are the same for the three quantifiers and can be synsetized by the transitional zone. In the conservative scenario $2.8 < E_r < 104.8$ and in the dissipative regime $3.6 < E_r < 123.0$.

We have found that the figures of H and C_{JS} have similar morphology but with a difference in scale. This is because the disequilibrium remains almost constant for all values of E_r in both scenarios, conservative and dissipative. Disequilibrium corresponding to the C_{LMC} complexity is also quasi-constant, but it has greater fluctuations around its mean value (conservative and dissipative regimes).

We conclude that the information quantifiers used in this work provide more details about the convergence process of the semiclassical system to the classical analogous, confirming the results obtained with the Poincaré sections used in Ref. [30], but with greater precision.

A Appendix

A.1 Semiclassical Model

Our semiclassical Hamiltonian is (1). In our methodology, the time evolution of all operator is the canonical one. The Hamiltonian also depends upon the classical variables A and P_A , which represent the reservoir. These classical quantities obey Hamilton's equations, of course, where the temporal generator is the mean value of the Hamiltonian [26, 49]. If we add to the system an appropriate ad hoc term we get dissipation [24, 25, 28].

Thus, for a given operator we have

$$\frac{d\hat{O}}{dt} = \frac{i}{\hbar} [\hat{H}, \hat{O}]. \quad (\text{A1})$$

The evolution of $\langle \hat{O} \rangle \equiv \text{Tr} [\rho \hat{O}(t)]$ is provided by

$$\frac{d\langle \hat{O} \rangle}{dt} = \frac{i}{\hbar} \langle [\hat{H}, \hat{O}] \rangle, \quad (\text{A2})$$

using a suitable density operator $\rho(0)$.
 $[\hat{H}, \hat{O}_i]$ can always be cast as [50, 51]

$$[\hat{H}, \hat{O}_i] = i\hbar \sum_{j=1}^q g_{ji} \hat{O}_j, \quad i = 0, 1, \dots, q, \quad (\text{A3})$$

where we can have $q \rightarrow \infty$. We are interested in finite q -values. In this case it is said that the set of operators \hat{O}_i , $i = 0, 1, \dots, q$, close a Lie semialgebra with \hat{H} [50, 51]. For a semiclassical Hamiltonian like (1), the coefficients g_{ji} depend on A and P_A . For classical variables one

$$\frac{dA}{dt} = \frac{\partial \langle \hat{H} \rangle}{\partial P_A}, \quad (\text{A4a})$$

$$\frac{dP_A}{dt} = -\frac{\partial \langle \hat{H} \rangle}{\partial A} - \eta P_A, \quad (\text{A4b})$$

where if $\eta > 0$ our system is dissipative. Instead, if $\eta = 0$, it is conservative. To verify these features [24, 25, 28] a particularly convenient space is used. We will call it “ v -space”. With respect to it, a bunch of equations deduced from Eqs. (A2) and (A4) conform an autonomous set of equations. They are first-order coupled differential ones, of the type [24, 25, 28]

$$\frac{d\vec{v}}{dt} = \vec{F}(\vec{v}), \quad (\text{A5})$$

with \vec{v} is a “vector”. It is regarded as a variable containing both classical and quantum parts. We consider volume elements V_S of this space, surrounded by a surface S . The dissipative η term generates a contraction of V_S [52]. The divergence of our vector is seen to be $-\eta$, given the fact that the matrix G in equations (A3) is traceless. This happens due to the canonical character of Eqs. (A1). Consequently, we must have [24, 25, 28]

$$\frac{dV_S(t)}{dt} = -\eta V_S(t). \quad (\text{A6})$$

Accordingly, we deal with a dissipative system [52]. If the classical Hamiltonian is of the form

$$H_{cl} = \frac{1}{2M} P_A^2 + V(A), \quad (\text{A7})$$

then the time-evolution of the total energy $\langle \hat{H} \rangle$ becomes

$$\frac{d\langle \hat{H} \rangle}{dt} = -\frac{\eta}{M} P_A^2. \quad (\text{A8})$$

Its meaning is to be ascertained through the lens of Eq. (A6) [24, 25, 28]. The complete set of equations (A2) + (A4) constitutes an autonomous set of non-linear coupled first-order ordinary differential equations (ODE). They allow for a dynamical description in which no quantum rules of the sub-quantal system are violated, e.g., the commutation-relations are trivially conserved at all times, since the quantum evolution is the canonical one for an effective time-dependent Hamiltonian (A and P_A , play the role of time-dependent parameters of the quantum system). The initial conditions are determined by a suitable quantum density operator $\hat{\rho}$. This happens both in the dissipative and in the conservative instances [27, 28].

References

- [1] Struyve, W. (2020). Semi-classical approximations based on Bohmian mechanics. *International Journal of Modern Physics A*, 35(14), 2050070.
- [2] Brack, M., & Bhaduri, R. (2018). *Semiclassical physics*. CRC Press.
- [3] Arndt, M., Hornberger, K., & Zeilinger, A. (2005). Probing the limits of the quantum world. *Physics world*, 18(3), 35.
- [4] Li, X. Q., Luo, J., Yang, Y. G., Cui, P., & Yan, Y. (2005). Quantum master-equation approach to quantum transport through mesoscopic systems. *Physical Review B*, 71(20), 205304.
- [5] Goan, H. S., & Milburn, G. J. (2001). Dynamics of a mesoscopic charge quantum bit under continuous quantum measurement. *Physical Review B*, 64(23), 235307.
- [6] Barker, J., & Bauer, G. E. (2019). Semiclassical thermodynamics of complex ferrimagnets. *Physical Review B*, 100(14), 140401.
- [7] Joos, E., Zeh, H. D., Kiefer, C., Giulini, D. J., Kupsch, J., & Stamatescu, I. O. (2013). *Decoherence and the appearance of a classical world in quantum theory*. Springer Science & Business Media.
- [8] Das, M. P. (2010). Mesoscopic systems in the quantum realm: fundamental science and applications. *Advances in Natural Sciences: Nanoscience and Nanotechnology*, 1(4), 043001.
- [9] Brandes, T. (2005). Coherent and collective quantum optical effects in mesoscopic systems. *physics reports*, 408(5-6), 315-474.
- [10] Iachello, F., & Zamfir, N. V. (2004). Quantum phase transitions in mesoscopic systems. *Physical review letters*, 92(21), 212501.
- [11] Guo, L. Z., Zheng, Z. G., & Li, X. Q. (2010). Quantum dynamics of mesoscopic driven Duffing oscillators. *Europhysics Letters*, 90(1), 10011.
- [12] Bloch, F. (1946). Nuclear induction. *Physical review*, 70(7-8), 460.
- [13] Milonni, P. W., Shih, M. L., & Ackerhalt, J. R. (1987). *Chaos in laser-matter interactions (Vol. 6)*. World Scientific Publishing Company.
- [14] Nielsen, S., Kapral, R., & Ciccotti, G. (2001). Statistical mechanics of quantum-classical systems. *The Journal of Chemical Physics*, 115(13), 5805-5815.
- [15] Micklitz, T., & Altland, A. (2013). Semiclassical theory of chaotic quantum resonances. *Physical Review E*, 87(3), 032918.
- [16] Cosme, J. G., & Fialko, O. (2014). Thermalization in closed quantum systems: Semiclassical approach. *Physical Review A*, 90(5), 053602.
- [17] Prants, S. V. (2017). Quantum-classical correspondence in chaotic dynamics of laser-driven atoms. *Physica Scripta*, 92(4), 044002.
- [18] Ribeiro, R. F., & Burke, K. (2018). Deriving uniform semiclassical approximations for one-dimensional fermionic systems. *The Journal of Chemical Physics*, 148(19).

- [19] Graefe, E. M., Höning, M., & Korsch, H. J. (2010). Classical limit of non-Hermitian quantum dynamics—a generalized canonical structure. *Journal of Physics A: Mathematical and Theoretical*, 43(7), 075306.
- [20] Bastarrachea-Magnani, M. A., Lerma-Hernández, S., & Hirsch, J. G. (2014). Comparative quantum and semiclassical analysis of atom-field systems. II. Chaos and regularity. *Physical Review A*, 89(3), 032102.
- [21] Allori, V., & Zanghì, N. (2009). On the classical limit of quantum mechanics. *Foundations of Physics*, 39, 20-32.
- [22] Kurchan, J. (2018). Quantum bound to chaos and the semiclassical limit. *Journal of statistical physics*, 171(6), 965-979.
- [23] Oliveira, A. C., Nemes, M. C., & Romero, K. F. (2003). Quantum time scales and the classical limit: Analytic results for some simple systems. *Physical Review E*, 68(3), 036214.
- [24] Kowalski, A. M., Plastino, A., & Proto, A. N. (1995). Semiclassical model for quantum dissipation. *Physical Review E*, 52(1), 165.
- [25] Kowalski, A. M., Plastino, A., & Proto, A. N. (1997). A semiclassical statistical model for quantum dissipation. *Physica A: Statistical Mechanics and Its Applications*, 236(3-4), 429-447.
- [26] Kowalski, A. M., Plastino, A., & Proto, A. N. (2002). Classical limits. *Physics Letters A*, 297(3-4), 162-172.
- [27] Kowalski, A. M., & Rossignoli, R. (2018). Nonlinear dynamics of a semiquantum Hamiltonian in the vicinity of quantum unstable regimes. *Chaos, Solitons & Fractals*, 109, 140-145.
- [28] Kowalski, A.M.; Plastino, A., Asger S. Thorsen (Ed.). (2020), *Semiquantum Time evolution. Classical limit*. Nova.
- [29] Kowalski, A. M., Plastino, A., & Gonzalez, G. (2021). Classical chaos described by a Density matrix. *Physics*, 3(3), 739-746.
- [30] Gonzalez Acosta, G., Plastino, A., & Kowalski, A. M. (2023). Dynamical classic limit: Dissipative vs conservative systems. *Chaos: An Interdisciplinary Journal of Nonlinear Science*, 33(1), 013126.
- [31] Kowalski, A. M., Martín, M. T., Plastino, A., & Rosso, O. A. (2007). Bandt–Pompe approach to the classical-quantum transition. *Physica D: Nonlinear Phenomena*, 233 (1), 21-31.
- [32] Kowalski, A. M., Martín, M. T., & Plastino, A. (2015). Generalized relative entropies in the classical limit. *Physica A: Statistical Mechanics and its Applications*, 422, 167-174.
- [33] Lopez-Ruiz, R., Mancini, H. L., & Calbet, X. (1995). A statistical measure of complexity. *Physics letters A*, 209(5-6), 321-326.
- [34] Lamberti, P. W., Martin, M. T., Plastino, A., & Rosso, O. A. (2004). Intensive entropic non-triviality measure. *Physica A: Statistical Mechanics and its Applications*, 334(1-2), 119-131.

- [35] Bandt, C., & Pompe, B. (2002). Permutation entropy: a natural complexity measure for time series. *Physical review letters*, 88(17), 174102.
- [36] Keller, K., & Sinn, M. (2005). Ordinal analysis of time series. *Physica A: Statistical Mechanics and its Applications*, 356(1), 114-120.
- [37] Rosso, O. A., Zunino, L., Pérez, D. G., Figliola, A., Larrondo, H. A., Garavaglia, M., & Plastino, A. (2007). Extracting features of Gaussian self-similar stochastic processes via the Bandt-Pompe approach. *Physical Review E*, 76(6), 061114.
- [38] Saco, P. M., Carpi, L. C., Figliola, A., Serrano, E., & Rosso, O. A. (2010). Entropy analysis of the dynamics of El Niño/Southern Oscillation during the Holocene. *Physica A: Statistical Mechanics and its Applications*, 389(21), 5022-5027.
- [39] Rosso, O. A., Olivares, F., Zunino, L., De Micco, L., Aquino, A. L., Plastino, A., & Larrondo, H. A. (2013). Characterization of chaotic maps using the permutation Bandt-Pompe probability distribution. *The European Physical Journal B*, 86, 1-13.
- [40] Aquino, A. L., Cavalcante, T. S., Almeida, E. S., Frery, A. C., & Rosso, O. A. (2015). Characterization of vehicle behavior with information theory. *The European Physical Journal B*, 88, 1-12.
- [41] Henry, M., & Judge, G. (2019). Permutation entropy and information recovery in non-linear dynamic economic time series. *Econometrics*, 7(1), 10.
- [42] Cao, Y., Tung, W. W., Gao, J. B., Protopopescu, V. A., & Hively, L. M. (2004). Detecting dynamical changes in time series using the permutation entropy. *Physical review E*, 70(4), 046217.
- [43] Zunino, L., Soriano, M. C., Fischer, I., Rosso, O. A., & Mirasso, C. R. (2010). Permutation-information-theory approach to unveil delay dynamics from time-series analysis. *Physical Review E*, 82(4), 046212.
- [44] Pessa, A. A., & Ribeiro, H. V. (2021). ordpy: A Python package for data analysis with permutation entropy and ordinal network methods. *Chaos: An Interdisciplinary Journal of Nonlinear Science*, 31(6).
- [45] Lopez-Ruiz, R. (2001). Complexity in some physical systems. *International Journal of Bifurcation and Chaos*, 11(10), 2669-2673.
- [46] Lin, J. (1991). Divergence measures based on the Shannon entropy. *IEEE Transactions on Information theory*, 37(1), 145-151.
- [47] Zunino, L., Soriano, M. C., & Rosso, O. A. (2012). Distinguishing chaotic and stochastic dynamics from time series by using a multiscale symbolic approach. *Physical Review E*, 86(4), 046210.
- [48] Rosso, O. A., Larrondo, H. A., Martin, M. T., Plastino, A., & Fuentes, M. A. (2007). Distinguishing noise from chaos. *Physical review letters*, 99(15), 154102.
- [49] Cooper, F., Dawson, J., Habib, S., & Ryne, R. D. (1998). Chaos in time-dependent variational approximations to quantum dynamics. *Physical Review E*, 57(2), 1489.
- [50] Alhassid, Y., & Levine, R. D. (1978). Connection between the maximal entropy and the scattering theoretic analyses of collision processes. *Physical Review A*, 18(1), 89.

- [51] Levine, R. D., Napoli, D. R., Otero, D., Plastino, A., & Proto, A. N. (1986). Maximum entropy approach to nuclear fission processes. *Nuclear Physics A*, 454(2), 338-358.
- [52] Arnold, V. I. (2013). *Mathematical methods of classical mechanics* (Vol. 60). Springer Science & Business Media.